IEEE Access
Multidisciplinary | Rapid Review | Open Access Journal

Received January 3, 2019, accepted January 14, 2019, date of publication January 21, 2019, date of current version March 4, 2019.

Digital Object Identifier 10.1109/ACCESS.2019.2893981

High Voltage Gain Ratio Isolated Resonant Switched-Capacitor Converter for Sustainable Energy

LEI YANG, (Member, IEEE), WENQIAN YU, (Student Member, IEEE), AND JIAXIANG ZHANG, (Student Member, IEEE)

School of Automation and Information Engineering, Xi'an University of Technology, Xi'an 710048, China

Corresponding author: Lei Yang (yanglei0930@gmail.com)

This work was supported in part by the China Postdoctoral Science Foundation under Grant 2018M643700, in part by the Scientific Research Project of Education Department of Shaanxi Province under Grant 18JS080, and in part by the Postdoctoral Research Grant Project of Shaanxi Province, China.

ABSTRACT A novel high-gain isolated two-switch boosting resonant switched-capacitor (ITBRSC) converter for sustainable energy is presented in this paper. It concludes a two-switch boosting resonant switched-capacitor (TBRSC) converter unit, an isolated transformer unit, and a load voltage regulation unit. There are two small value inductors in the proposed topology. They are, respectively, injected into the charge loop and the discharge loop. As a result, the pulsating input current is highly decreased. In this way, it could achieve the continuous input current in the primary side of ITBRSC converter. The TBRSC converter unit boosts the input voltage with the high gain ratio. In combination with the transformer, the ITBRSC converter could provide a good isolation performance by adopting the transformer. The proposed converter in this paper could be used in the variable input voltage and wide operation area. It could be acted as the high-gain isolated power supply for sustainable energy systems, such as electric vehicles and wind energy. The SC converter-based high-gain isolated converter could achieve the high power density and simple topology. A 500-W power-rating ITBRSC converter is constructed. The function of the ITBRSC converter is demonstrated and tested with the simulation and experiments. The high gain ratio and robust performance of the proposed converter are totally verified. It could facilitate the application of SC converters for sustainable energy.

INDEX TERMS Isolated two-switch boosting resonant switched capacitor (ITBRSC) converter, high gain, sustainable energy, high-power density.

I. INTRODUCTION

The isolated high voltage gain ratio DC-DC converters have been widely used for the power supply applications. The sustainable energy applications such as the solar photovoltaic (PV), full electric and hybrid vehicles applications which require the high voltage gain ratio DC-DC converters [1], [2]. In the automotive applications, the battery voltage should be boosted with the high gain ratio to provide the voltage for the inverter of the motor unit [2], [3]. The same thing will have happened in the solar energy system. The output voltage of the fuel cell stacks, the photovoltaic arrays, and the supercapacitors are low. As a result, the low output voltage should be increased to a high voltage for the normal applications [4]. For the traditional charger of the electric vehicles, the inductor-based DC-DC converter is used for the DC voltage adjustment and the full-bridge or half-bridge circuit is acted as the inverter unit. However, for the traditional inductor-based DC-DC converter such as boost converter, the bulky and large volume magnetic elements have been added in the circuit. As a result, the power density of the traditional DC-DC converter is low. What's more, for the high-power application, the price is high. To reduce the noise and to satisfy the safety requirements, the power system will use the isolation element. The isolation element is usually the transformer. The voltage conversion ratio always depends on the turns ratio between the primary side and the secondary side of the transformer.

As no participation of magnetic components such as the transformer and the inductor [5]–[7], switched capacitor (SC) converters has been widely used for the advanced requirements of high-power density, light weight and so on. Compared to the traditional inductor-based converters,

this special characteristic inspires the capacity for full monolithic integration and small volume [8]–[10]. SC converters employ only switches and capacitors, with the rapid development of the wide-band gap devices and the capacitors, the advantages of SC converters will be boosted. The power transfer of SC converters is achieved by controlling the charging process and discharging process of the flying capacitor [6]. SC converters have the wide applications area which ranges from mW chip integration [11]–[18] to kW high-power applications [19]–[26]. In order to achieve the output voltage regulation, several kinds of control method have been used on SC converters such as pulse width modulation (PWM), variable frequency control, phase-shift control and variable structure control. SC converters have the wide range of applications including the LED driver [27]–[30], battery balancing applications [31], energy buffering [32], electric vehicles [20], [26], [33], [34], and energy harvesting systems [33]. Paper [29] presents a 2W SC converter based LED driver with the frequency modulated control method. The average current of SC converters has a directional relationship of the input voltage and the LED forward voltage as shown in [29]. The SC converter-based LED driver in [30] adds an inductor in the SC circuit. As a result, the LEDs load power which is transferred from the power source does not depend on the forward voltage of LEDs. The energy efficiency of the traditional converter is highly increased. When it comes to the high-power applications, a 55-kW variable 3X SC converter for automotive vehicles is invented and demonstrated in paper [20]. These four variable level SC converters could highly improve the power density of the converter by dramatically reducing the inductance requirement, compared with the general inductor-based converter. This converter could be operated in wide voltage conversion ratio range with the high energy efficiency.

The resonant switched capacitor (RSC) converters are invented to overcome the disadvantages of SC converters (the high pulsating currents and the high switching loss) in the charge loop and discharge loop of SC converters [26], [27]. The pulsating charging current and the voltage stress of circuit could be reduced by injecting the inductive element such as the small value inductor [30]. A 1kW power level two-switch boosting switched-capacitor (TBSC) converter is presented in [35]–[38]. It provides high efficiency (97.5% peak efficiency). What's more, it provides soft rising edge input current to increase the energy efficiency and reduce the EMI noise. In paper [35], the charge-balance transient-calculation (CT) modeling method is adopted to build the model for SC converter. To regulate the load voltage, the proportional–integral (PI) control method is used. With the linear control method, the regulation performance is not good enough with the slow dynamic response speed. In order to improve the output voltage regulation performance for the TBSC converter, a nonlinear variable frequency one-cycle control method is proposed in [38].

However, all these SC converters which mentioned in the above papers are the non-isolated topologies.

Papers [39]–[42] provides different kinds of isolated SC converters to extend the application range of SC converters. The isolated SC converter in [39]–[40] is acted as an auxiliary power supply in the automotive vehicle applications. It controls the power which flows from the high voltage part to the low voltage part. It provides the directional power-flow, small voltage stress, and small turns ratio of the transformer. What's more, the wide bandgap devices are used in this quasi-SC converter to provide the low switching loss. Paper [41] presents a high energy efficiency, high voltage conversion ratio SC converter. The proposed converter in [41] has consisted of a fly-back circuit and an isolated SC converter cell. It achieves high cost-effective advantage for the extreme operation. However, its high voltage gain ratio of topology in [41] depends on the high or low turns ratio of designed transformer. What's more, the high pulsating input current will be occurred in the charging loop. In order to solve the aforesaid problems of the isolated high gain ratio converter, this paper proposes a high gain ratio isolated two-switch boosting resonant switched-capacitor (ITBRSC) converter. The research in this paper is based on the previous work on the TBSC converter as shown in [35]–[38] and [43]. The proposed converter includes three stages. The first stage is the high gain TBRSC converter. The second stage is the isolated transformer, and the third stage is the load voltage regulation circuit. The proposed high gain ratio ITBRSC converter could be used in the high gain ratio and isolation condition. With the small value inductor, the input current is operated in the continuous condition. With the SC converter which is composed only the switches, capacitors and small value inductor, the power density of isolated converter could be highly improved. The isolated SC converter proposed in this paper could work in the wide operation range with the robust performance. It could be wildly used for the sustainable energy system with the requirements of high-power density, high voltage gain ratio and good isolation. In this paper, the detailed operation analysis and the performance verification of the ITBRSC converter is presented in this paper. The rest of this paper is organized as follows: the topology and operation theory of the ITBRSC converter is provided in section II. In section III, the model and calculation are presented. The simulated and the experimental results are shown in section IV. Section V shows the conclusions and discussions.

II. DESCRIPTION AND OPERATION PRINCIPLES

Fig.1 shows the designed ITBRSC converter. It can be seen timing waveforms in Fig.2. Fig.3 shows the four equivalent operation states in the different timing periods. The operation analysis will be conducted in the wide input voltage range and different load power levels. The left part of the proposed isolated SC converter is the resonant TBSC (TBRSC) circuit. It is derived by optimizing the TBSC converter in [35]–[38] and [43]. It introduces two small value inductors in the charge loop and the discharge loop for TBSC converter, respectively. As a result, this SC converter could work stably

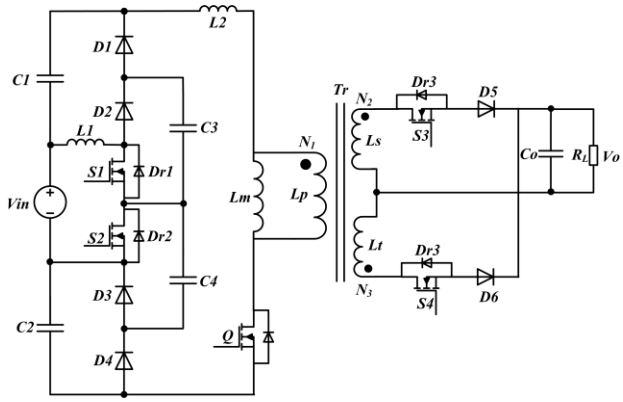

FIGURE 1. Topolog of the proposed converter.

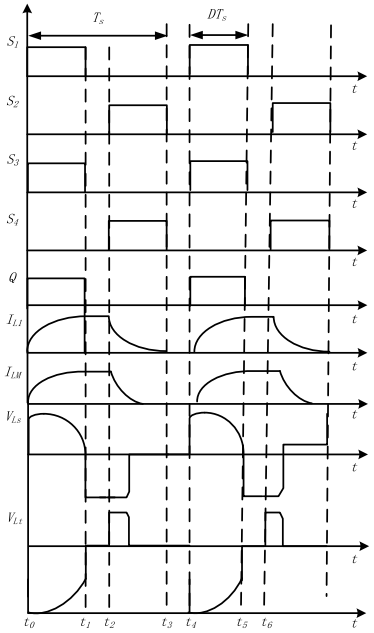

FIGURE 2. Steady-stat waveforms of proposed circuit.

without the high peak spikes in the input current. The middle part of the proposed converter is the transformer which could be used as the isolation unit. The right part of the proposed isolated SC converter is the regulation circuit to provide the load power. S_1 – S_4 and Q share the same duty-cycle D. One cycle time is set T_{sq}. Switches S_1, S_3 and Q share the same driving signals ($U_{s1} = U_{s3} = U_q$). While, the driving signals for switches S_2, S_4 are U_{s2} and U_{s4}(U_{s2}= U_{s4}). The two groups control signals work complementarily with each other. There are four equivalent operation states as shown in Fig.2 and Fig.3.

Fig.1 shows the State 1 during the time period t_0-t_1. In this time period, the control signal turns on the S_1, S_3 and Q. While, S_2 and S_4 are turned off. The power source transfers the energy to the capacitor C_4 during DT_s time period. On the other hand, capacitor C_1 is charged by the capacitor C_1. The power source, capacitors C_1 and C_2 are connected in series

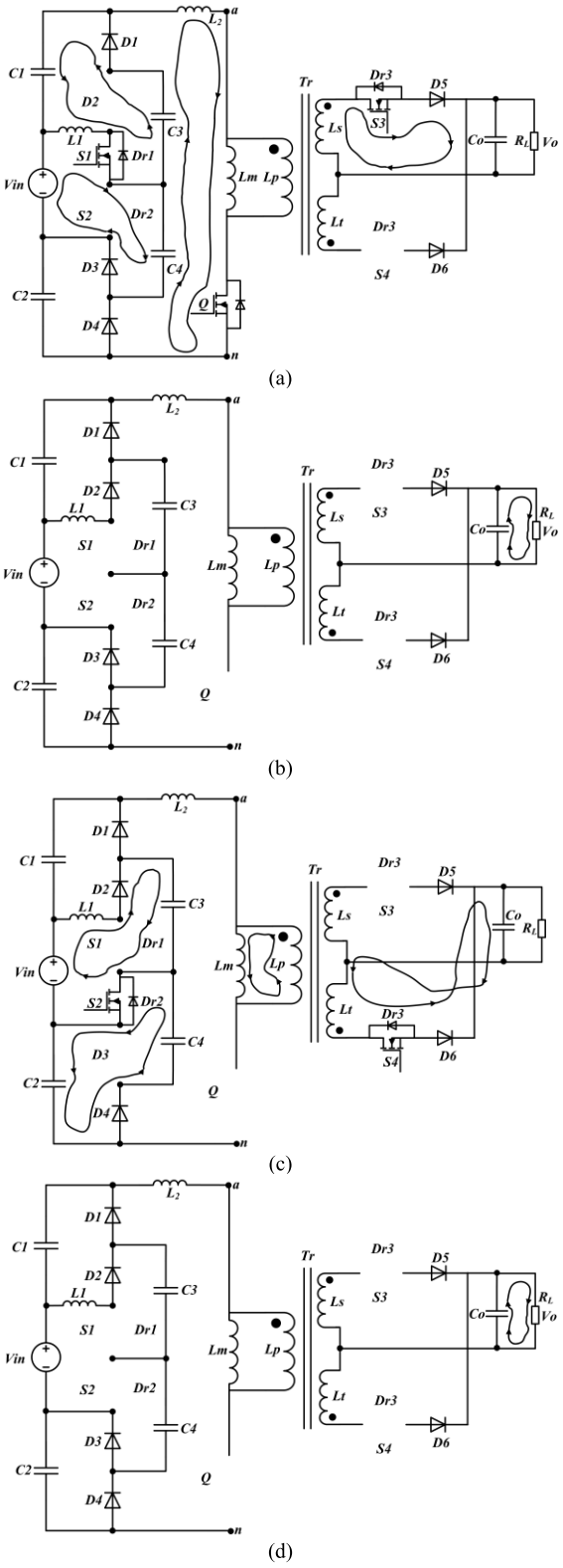

FIGURE 3. Equivalent operation states of proposed circuit (a) State 1[t_0, t_1]. (b) State 2[t_1, t_2]. (c) State 3[t_2, t_3]. (d) State 4[t_3, t_4].

in the proposed topology. They continuously deliver their energy to transformer T_r in state 1. In the same time period, the load power is maintained by L_s.

Fig.1(b) shows the State 2 during the time period $t_1 - t_2$. In this time period, the control signal turns off all switches. The load power is maintained by the filter capacitor C_o.

Fig.3(c) shows the State 3 during the time period $t_2 - t_3$. In this time period, the control signal turns on S_2 and S_4. While S_1, S_3 and Q are turned off. The power source transfers its energy to capacitor C_3 in the DT_s time period. On the other hand, capacitor C_2 is charged by capacitor C_4. L_m is continuously charged by L_p during this time period. The load power is maintained by L_t .

Fig.3(d) shows the State 4 during the time period $t_3 - t_4$. In this time period, the proposed isolated SC converter works similarly as State 2.

The operation states and the circuit calculation are complex. To make the simple analysis, the assumptions are made as follows: (a) S_1, S_2, S_3, $S_4$and Q are the ideal switches. They share the same internal resistance ($R_{s1} = R_{s2} = R_{s3} = R_{s4} = R_{sq}$). (b) Capacitors C_1, C_2,C_3 and C_4 are ideal. They share the same capacitance ($C_1 = C_2 = C_3 = C_4 = C$). What's more, they also have the same equivalent series resistance(ESR) in the charging and discharging periods ($R_{c1} = R_{c2} = R_{c3} = R_{c4} = R_c$). (c) D_1, D_2,D_3, D_4, D_5 and D_6 are identical with the same internal resistance ($R_{d1} = R_{d2} = R_{d3} = R_{d4} = R_{d5} = R_{d6} = R_d$) (d) In the calculation, the forward voltage of diodes D_1, D_2,D_3, D_4, D_5 and D_6 is set zero. The internal resistance of power source is ignored. (e) There are two groups control signal. One is for S_1, S_3 and Q and the other group is for S_2 and S_4. When S_1, S_3 and Q are turned on, S_2 and S_4 should be turned off and vice versa. (f) The one cycle time of transistors is set T_{sq} and f_{sq} is the corresponding switching frequency. (g) The duty-cycle D of switches $S_1 - S_4$ and Q is less than 0.5. (e) In the Fig.1 and Fig.3, L_m represents the magnetic inductance of transformer, L_p represents the equivalent inductance of primary side of transformer, L_s and L_r are respectively represent the equivalent inductance of two different secondary side of the transformer. The turns ratio of the transformer is set N_{Lp}:N_{Ls}:$N_{Lt} = N_1$:N_2:N_3.

III. MODEL AND ANALYSIS OF THE PROPOSED ISOLATED SC CONVERTER

Different modeling methods have been proposed for SC converter [44]–[48]. Papers [44] and [45] present a state-space averaging (SSA) model. It is usually used for the inductor-based converter. Based on the model of equivalent output resistance, the prediction of SC converter is reached. By including the duty-cycle and frequency, the equivalent output impedance is constructed in [46] and [47] which is called the average-current based conduction loss model. Paper [48] proposes a slow and fast switching limit model. It builds the equivalent output impedance model in the slow switching frequency area or fast switching frequency area. By considering different parameters, a charge-balance transient calculation model is derived in [37]. However, all the models mentioned above are the steady-state model. In the operation of SC converter, it also needs to consider the dynamic behaviors [49]. A new dynamic modeling method is shown in in [50]–[52]. It is invented based on the switching "on time" and the switching "off time" instead of duty-cycle of a transistor. In the wide operation range, it could provide the accurate transient and steady-state prediction of TBSC converter. By adopting this modeling method, a novel variable frequency one cycle control method is proposed, which highly improves the dynamic response speed in the wide operation range [51], [52]. The dynamic volt-second balance principle is adopted in this paper. The different dynamic parameters of ITBRSC converter are considered. The primary side of the transformer and the secondary side of the transformer are calculated, separately.

In one cycle, the input voltage, voltage of capacitor C_3 and voltage of capacitor C_4 have an instantaneous relationship as:

$$\begin{aligned} V_{in} + V_c(t) &= V_{c3}(t) + V_{c4}(t) \\ &= V_{c3max} + V_{c3min} = V_{c4max} + V_{c4min} \end{aligned} \tag{1}$$

where $V_{c(t)}$ is the real time voltage of C_1 or C_2, $V_{c3(t)}$ is real time voltage of C_3, $V_{c4(t)}$ is real time voltage of C_4. In one cycle time period,V_{c3max} represents the maximum voltage of C_3, V_{c3min} represents the minimum voltage of C_3, V_{c4max} represents the maximum voltage of C_4, and V_{c4min} represents the minimum voltage of C_4.

V_{an} is the tested voltage between the point a and point n as shown in Fig.3. It can be derived as:

$$V_{an} = V_{c3max} + V_{c3min} + V_{in} = V_{c4max} + V_{c4min} + V_{in} \tag{2}$$

During the state $1[t_0 - t_1]$ as shown in Fig.3 (a), there are three loops of the left part of the proposed isolated SC converter as shown in Fig.3(a). By considering the KVL, the equations could be written as:

$$-L_1 \frac{di_{L1}(t)}{dt} + V_{c3}(t) - V_{c1}(t) = 0 \tag{3}$$

$$V_{in} - L \frac{di_{L1}(t)}{dt} - V_{c4}(t) = 0 \tag{4}$$

$$V_{in} + V_{c1}(t) + V_{c2}(t) - L_m \frac{di_{Lm}(t)}{dt} = 0 \tag{5}$$

where $V_{c1(t)}$ is the real time voltage of C_1.

The capacitance of capacitor C_3 is equal to capacitance of capacitor C_4. Based on the KCL, the following equation could be achieved.

$$C_3 \frac{dv_{c3}(t)}{dt} = C_4 \frac{dv_{c4}(t)}{dt} = -0.5 i_{L1}(t) \tag{6}$$

By submitting (3), (5) and (6) into (4), it can get the relationship as:

$$\begin{aligned} V_{c4}(t) = V_{in} &- (V_{in} - V_{c4}(t_0)) \cos 2\pi f_{lc}(t - t_0) \\ &+ \sqrt{\frac{L_1}{C_4}} I_{L1}(t_0) \sin 2\pi f_{lc}(t - t_0) \end{aligned} \tag{7}$$

By submitting (3)-(5) into (6), the equation can be derived as:

$$i_{L1}(t) = (I_{L1}(t_0)\cos 2\pi f_{lc}(t-t_0) + (V_{in} - V_{c4}(t_0))\sqrt{\frac{2C_4}{L_1}}\sin 2\pi f_{lc}(t-t_0)) \quad (8)$$

where f_{lc} is the resonant frequency $f_{lc} = \frac{1}{2\pi\sqrt{L_1 C_4}}$.

When it comes to the secondary side of the proposed isolated SC converter, considering the KVL and the KCL, the two equations can derive as:

$$V_o + V_d - L_s\frac{di_{Ls}}{dt} = 0 \quad (9)$$

$$i_{Ls}(t) = I_0 = \frac{V_o(t)}{R_L} \quad (10)$$

where $i_{Ls}(t)$ represents the real time current which flows through inductor L_s.

During time period $[t_0 - t_1]$, the magnetic flux $\emptyset$ of the transformer can be written as:

$$N_1\frac{d\emptyset}{dt} = V_{in} \quad (11)$$

The magnetic flux increases in State 2 and it can be derived as:

$$\Delta\emptyset_p = \frac{V_{an}}{N_1}D_2 T_{sq} \quad (12)$$

where T_{sq} is one cycle time.

The real time current of inductor L_p in the primary side of transformer can be presented as:

$$i_{p(t)} = \frac{V_{an}}{(L_2 + L_m)}t \quad (13)$$

The voltage of L_s is derived as:

$$V_{o1} = \frac{N_2}{N_1}V_{an} \quad (14)$$

During the time period $[t_1 - t_2]$, considering the KVL, it can derive the following equation as:

$$L_m\frac{di_{L_m}(t)}{dt} = -L_p\frac{di_p(t)}{dt} \quad (15)$$

what's more, by using KCL, the real time current of L_m and the real time current L_p have the relationship as:

$$i_{Lm}(t) = -i_{Lp}(t) \quad (16)$$

During the State 3 $[t_2, t_3]$ as shown in Fig.3 (c), by considering the KCL, the following equations can be written as:

$$V_{c4}(t) - V_{c2}(t) - V_d = 0 \quad (17)$$

$$V_{in} - L_1\frac{di_{L1}(t)}{dt} - V_{c3}(t) - V_d = 0 \quad (18)$$

In the discharge loop of capacitor C_4, it can get the equation based on the KCL as:

$$C_4\frac{dV_{c4}(t)}{dt} = -C_2\frac{dV_{c2}(t)}{dt} \quad (19)$$

When switch S_4 is turned on, in the discharge loop of secondary side of transformer L_t, the following two equations can be written as:

$$V_o + V_d - L_t\frac{di_{Ls}(t)}{dt} = 0 \quad (20)$$

$$i_{Lt}(t) = I_0 = \frac{V_o(t)}{R_L} \quad (21)$$

where $i_{Lt}(t)$ is the real time current L_t.

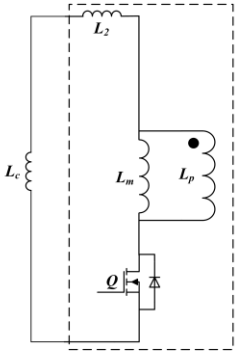

FIGURE 4. Equivalent primary side inductor of the proposed isolated SC converter.

As shown in Fig.4, the equivalent primary side inductance of the proposed isolated SC converter could be drawn as:

$$L_r = \frac{(L_c + L_2 + L_m)L_p}{L_c + L_2 + L_m + L_p} \quad (22)$$

where L_c is the equivalent inductance of the TBRSC converter, and L_p is the inductance of primary side of the transformer.

It can be seen in Fig.4, the resonant frequency of equivalent primary side can be written as:

$$f_r = \frac{1}{2\pi\sqrt{L_r(C_3 + C_4)}} \quad (23)$$

and,

$$T_r = 2\pi\sqrt{L_r(C_3 + C_4)} \quad (24)$$

Based on equation (24), the following conclusions could be made:

If the $T_r > DT_s$, the proposed converter works under the CCM operation mode.

If the $T_r = DT_s$, the proposed converter works under the BCM operation mode.

If the $T_r < DT_s$, the proposed converter works under the DCM operation mode.

A. CCM CALCULATION

In the CCM, the secondary side voltage of the proposed isolated SC converter could be derived as:

$$V_s = V_t = \frac{N_2}{N_1}V_{an} = \frac{N_3}{N_1}V_{an} \quad (25)$$

where V_s and V_t respectively represents the voltage of the secondary side L_s of the transformer and the voltage of secondary side L_t of the transformer.

The current of L_p and the input voltage have the relationship as:

$$\frac{di_p}{dt} = \frac{V_{in}}{L_m} \tag{26}$$

The maximum current of L_p could be derived as:

$$I_{pmax} = I_{pmin} + \frac{V_{in}}{L_m} \times D \times T_{sq} \tag{27}$$

The current of L_t and the load voltage have the relationship as:

$$\frac{di_t}{dt} = \frac{V_o}{L_t} \tag{28}$$

The maximum current of L_t is presented as:

$$I_{tmax} = I_{tmin} + \frac{V_{in}}{L_t} \times \mathrm{D} \times T_{sq} \tag{29}$$

During the time period of State 1, the increase of magnetic flux of the primary side L_p is written as:

$$\Delta\emptyset_{p(+)} = \frac{(V_{in} + V_{c3} + V_{c4})}{N_1} DT_{sq} \tag{30}$$

In the first half switching cycle (stage 1 and stage 2), the load voltage of the proposed isolated SC converter can be simply presented as:

$$V_{o1} = 2D\frac{N_2}{N_1}(V_{in} + V_{c3} + V_{c4}) \tag{31}$$

During the time period of State 3 and State 4, the decrease of magnetic flux of the primary side L_p is written as:

$$\Delta\emptyset_{p(-)} = \frac{(V_{in} + V_{c3} + V_{c4})}{N_3}(T_r - DT_{sq}) \tag{32}$$

In the second half switching cycle (stage 3 and stage 4), the load voltage of the proposed isolated SC converter is calculated as:

$$V_{o2} = 2\frac{(V_{in} + V_{c3} + V_{c4})}{T_{sq}}(T_r - DT_{sq}) \tag{33}$$

The average output voltage of the proposed isolated SC converter in one switching cycle could be written as:

$$\mathrm{V_o} = \frac{(\mathrm{V_{o1}} + \mathrm{V_{o2}})}{2} = (\mathrm{V_{in}} + 2\bar{V_c})(\mathrm{T_r} f_{sq} + D\frac{\mathrm{N_2}}{\mathrm{N_1}} - D) \tag{34}$$

where $\bar{V_c}$ represents the average voltage of capacitor C_3 or C_4 in one switching cycle.

It can be seen from (34), in the CCM condition, the voltage gain ratio of the proposed converter is in the direct proportion to the switching frequency of switch Q.

B. BCM CALCULATION

In the BCM, the maximum current of L_t can be written as:

$$I_{tmax} = \frac{N_1}{N_2}\frac{V_{an}}{L_m f_s} D \tag{35}$$

Considering the equation (35), the output current is written as:

$$I_o = 0.5 I_{tmax} \times D \tag{36}$$

Based on the equations (35) and (36), the boundary load current can be derived as:

$$I_{oG} = I_o = \frac{V_{in}}{2L_m f_{sq}}\frac{N_1}{N_2} D^2 \tag{37}$$

When D = 0.5, the maximum output current could be written as:

$$I_{oGmax} = \frac{N_1}{N_2} \times \frac{V_{in}}{8L_m f_{sq}} \tag{38}$$

By considering equations (35)-(38), the maximum output current could be rearranged as:

$$I_{oG} = 4I_{oGmax} \times D \tag{39}$$

In State 1, the increased magnetic flux of L_p could be written as:

$$\Delta\emptyset_{p(+)} = \frac{(V_{in} + V_{c3} + V_{c4})}{N_1} DT_{sq} \tag{40}$$

In the first half switching cycle (State 1 and State 2), the output voltage of the proposed isolated SC converter could be derived as:

$$V_{o1} = 2D\frac{N_2}{N_1}(V_{in} + V_{c3} + V_{c4}) \tag{41}$$

In State 3 and State 4, the decreased magnetic flux of the primary side L_p could be written as:

$$\Delta\emptyset_{p(-)} = \frac{(V_{in} + V_{c3} + V_{c4})}{N_3} T_r \tag{42}$$

In the second half switching cycle (State 3 and State 4), the load voltage of the proposed isolated SC converter can be presented as:

$$V_{o2} = 2\frac{(V_{in} + V_{c3} + V_{c4})}{T_{sq}} T_r \tag{43}$$

The average load voltage of the proposed isolated SC converter in one switching cycle is presented as:

$$\mathrm{V_o} = \frac{(\mathrm{V_{o1}} + \mathrm{V_{o2}})}{2} = (\mathrm{V_{in}} + 2\bar{V_c})(\frac{\mathrm{T_r}}{\mathrm{T_{sq}}} + D\frac{\mathrm{N_2}}{\mathrm{N_1}}) \tag{44}$$

As shown in (44), in the BCM condition, the load voltage gain ratio increases with the rising of f_{sq} and D.

C. DCM CALCULATION

In the DCM, the voltage conversion ratio has a relationship to the D and I_o. The increased magnetic flux of the primary side is equal to the decreased magnetic flux of the secondary side. In part of the DT_s time period, the current of L_s or L_t is zero. Setting the time period that the current of L_s or L_t over zero is ΔDT_s. The magnetic flux balance could be written as:

$$\Delta\emptyset_p = \Delta\emptyset_t = \frac{V_{an}}{N_1}D = \frac{V_o}{N_3}\Delta D \tag{45}$$

Then the duty-cycle ΔD could be derived as:

$$\Delta D = \frac{V_{an}}{V_o} \times \frac{N_3}{N_1}D \tag{46}$$

The maximum current of L_t in one switching cycle is shown as:

$$I_{tmax} = \frac{V_o}{L_t} \times \Delta D \times T_{sq} \tag{47}$$

The load current of the proposed isolated SC converter could be drawn as:

$$I_o = 0.5 \times I_{tmax} \times \Delta D \tag{48}$$

In the loop of the load regulation circuit, the load current of the proposed isolated SC converter could be presented as:

$$I_o = \frac{V_o}{R_L} \tag{49}$$

Submitting (46)-(49) into (45), the equation (45) could be arranged as:

$$V_{o1} = V_{an} \times \frac{N_3}{N_1}D\sqrt{\frac{R_L}{2L_t f_{sq}}} \tag{50}$$

Assuming the transformer T_r is ideal. As shown in [43] and [44], the power of TBSC converter will be firstly stored in C_3. Then, it will be transferred to the load. As a result, the following equation could be derived as:

$$C_3\,(V_{c3max} - V_{c3min}) = \frac{V_o}{R_L} \times \frac{1}{f_{sq}} \tag{51}$$

Considering the volt-second balance principle, in second half switching cycle, the load voltage can be presented as:

$$V_{02} = V_{an} \times \left(\frac{N_2}{N_1}D + \frac{N_3}{N_1}D\sqrt{\frac{R_L}{2L_t f_{sq}}}\right) \tag{52}$$

and the voltage V_{an} could be presented as:

$$V_{an} = V_{in} + V_{c3max} + V_{c3min} = V_{in} + V_{c3max} + V_{c3min} \tag{53}$$

Letting $V_{c3max} + V_{c3min} = 2\bar{V}_c$, the equation (53) could be rearranged as:

$$V_{an} = V_{in} + 2\bar{V}_c \tag{54}$$

TABLE 1. Circuit parameters for ITBRSC converter.

Component	Type	Value
Input Voltage	/	24V
S_1,S_3 and S_4(FQA40N25)	N-channel	40A,250V,$R_{DS(0n)}$=70mΩ
S_2(IRFB4332PBF)	N-channel	60A,250V,R_{DS}=29mΩ
Q(FDP20N50)	N-channel	20A,500V, $R_{DS(0n)}$=200mΩ
$D_1 - D_6$	High efficiency ultrafast diode	I_F=30A,V_{PRM}=200V,t_{rr}=22ns, Rd=10mΩ
$C_1 - C_4$	Film Capacitor	450V,100uF
C_o	Film Capacitor	450V,330uF
L_1	Inductance	10uH
L_2	Inductance	10uH
L_M	Magnetic Inductance	200uH
T_r	Transformer	N_1=5,N_2=N_3=10

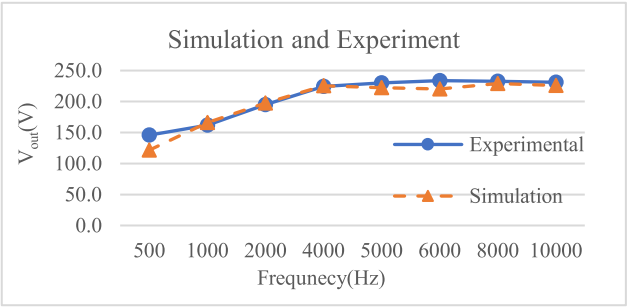

FIGURE 5. Vout with variable frequency and 500Ω load resistance.

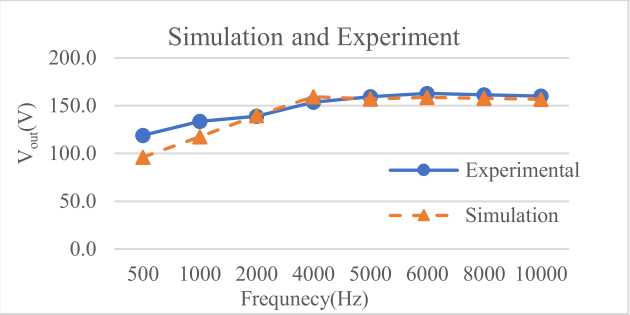

FIGURE 6. Vout with variable frequency and 250Ω load resistance.

where V_c is the voltage of capacitor C_1 or C_2, V_{cmax} is the maximum voltage of capacitor C_1 or C_2, and V_{cmin} is the minimum voltage of capacitor C_1 or C_2.

Considering equations (50)-(54), the average output voltage of the proposed isolated SC converter can be shown as:

$$V_o = (V_{in} + 2\bar{V}_c) \times \left(\frac{N_2}{N_1}D + \frac{N_3}{N_1}D\sqrt{\frac{R_L}{2L_t f_{sq}}}\right) \tag{55}$$

It can be seen from (55), in the DCM condition, the load voltage gain ratio of the proposed isolated SC converter is in the inverse proportion to the switching frequency of switch Q and in the direct proportion to the duty-cycle of D.

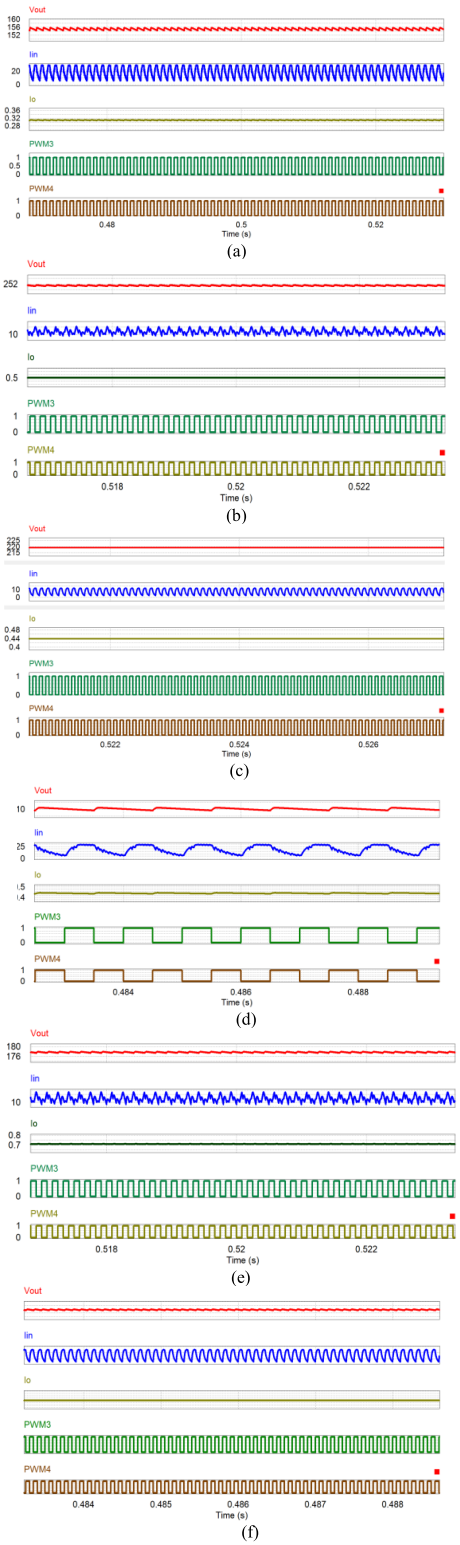

FIGURE 7. Waveforms of V_{out}, I_{in}, I_o, PWM3 and PWM4 signals, under R_L = 500ohm and R_L = 250 ohm. (a) f_{sq} = 1kHz and RL = 500ohm. (b) f_{sq} = 6kHz and R_L = 500ohm. (c) f_{sq} = 10kHz and R_L = 500ohm. (d) f_{sq} = 1kHz and R_L = 250ohm. (e) f_{sq} = 6kHz and R_L = 250ohm. (f) f_{sq} = 10kHz and R_L = 250ohm.

IV. SIMULATION AND EXPERIMENT VERIFICATION

In this paper, the simulation and experiments are both conducted to test the performance of the proposed isolated

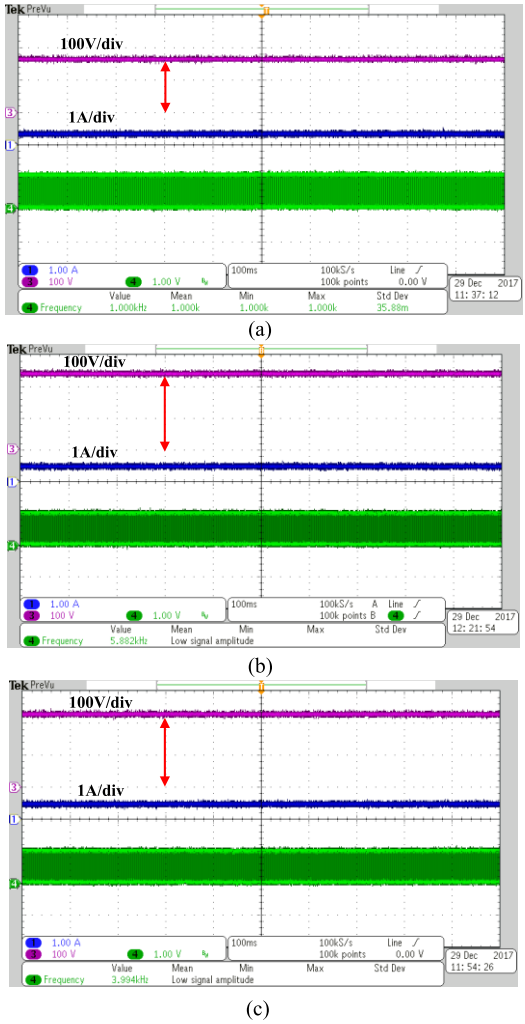

FIGURE 8. Waveforms of V_{out}, I_o and PWM signal of S_3 with variable switching frequency (1kHz, 6kHz and 10kHz) and 500Ω load resistance. (a) 1kHz. (b) 6kHz. (c)10kHz.

SC converter. The power level of the experimental ITBRSC converter is 500W. The input voltage is set 24V which is provided by a 1kW DC power source. The detailed parameters of the proposed converter can be seen in Table 1. The steady-state performance and the dynamic performance are respectively presented in this paper with the open-loop control method. The proposed isolated SC converter works in the different load resistance conditions and switching frequency. The switching frequency of transistors $S_1 - S_4$ and Q is set between 500Hz-10kHz. The duty-cycle D of transistors are 0.5. The voltage conversion ratio is measured with the variable switching frequency. The experimental results are compared with the simulated results. The boundary switching frequency is set 6kHz (the boundary condition equivalent primary side inductance of the proposed ITBRSC converter is 3.52uH). The primary target of this paper is to propose a novel high gain ratio isolated SC converter and to verify the theory analysis, as a result, the switching frequency is not high enough. The high switching frequency and high-power

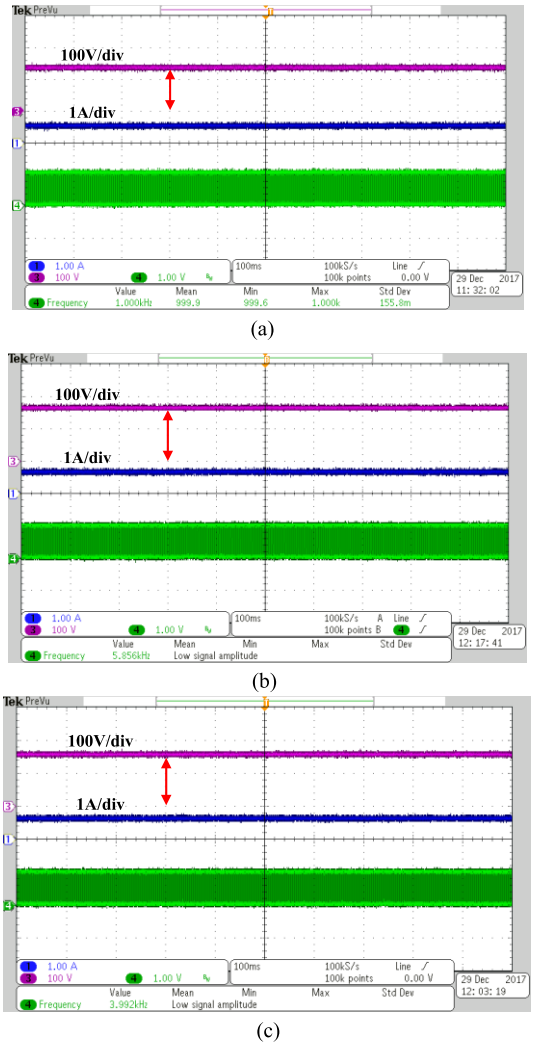

FIGURE 9. Waveforms of V_{out}, I_o and PWM signal of S_3 with variable switching frequency (1kHz, 6kHz and 10kHz) and 250Ω load resistance. (a) 1kHz. (b) 6kHz. (c) 10kHz.

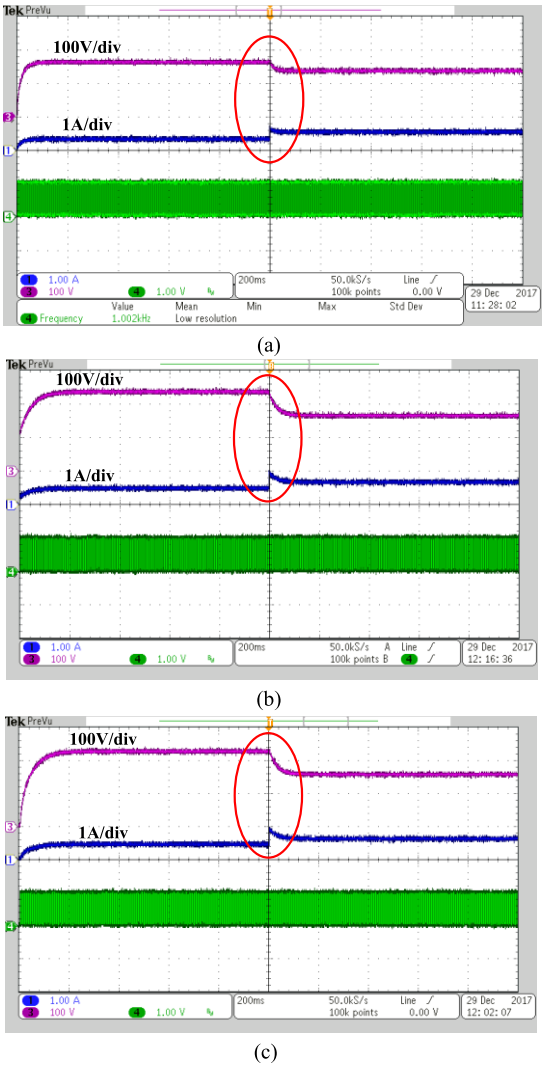

FIGURE 10. Waveforms of V_{out}, I_o and PWM signal of S_3 with variable switching frequency (1kHz, 6kHz and 10kHz) and load resistance step-down 500-250Ω. (a) 1kHz. (b) 6kHz. (c) 10kHz.

high gain ratio isolated SC converter will be presented in the future work.

A. COMPARISON OF SIMULATION AND EXPERIMENTAL RESULTS

The experiments and simulation are conducted with variable switching frequency and load resistance. Considering the parameter of ITBRSC converter, the 6kHz boundary switching frequency is set. The comparison results are shown as Fig.5 and Fig.6. It shows that, at the same switching frequency, the voltage gain ratio will be lower than at heavier load. Below the boundary switching frequency 6kHz, the voltage gain ratio of the proposed isolated SC converter will climb with the growing of the switching frequency. In contrast, if the proposed isolated SC converter works over the boundary switching frequency, with the rising switching frequency, the voltage gain ratio of the proposed isolated SC converter will decrease. The measured maximum voltage gain ratio is close to 10. Being affected by the circuit stray inductance, the simulated voltage gain ratio line of the ITBRSC converter is little different from the experimental results with the same load power and same switching frequency. The simulated results generally have a good match with the experimental results.

B. SIMULATION VERIFICATION OF THE ITBRSC MODEL

The steady-state performance of ITBRSC converter is tested in the load resistance 250Ω and 500Ω, respectively. The tested switching frequency are 1kHz, 6kHz and 10kHz. The simulated results of the load voltage, input current, load current, control signals of PWM3 for switch S_3 and PWM4 for switch S_4, and the load voltage are presented in Fig.7. As shown in Fig.7 that, with the same switching frequency, the voltage gain ratio in the 500Ω load resistance condition is higher than that in the 250Ω load resistance condition. The output voltage ripple could be reduced by increasing the switching frequency of switches S_3 and S_4.

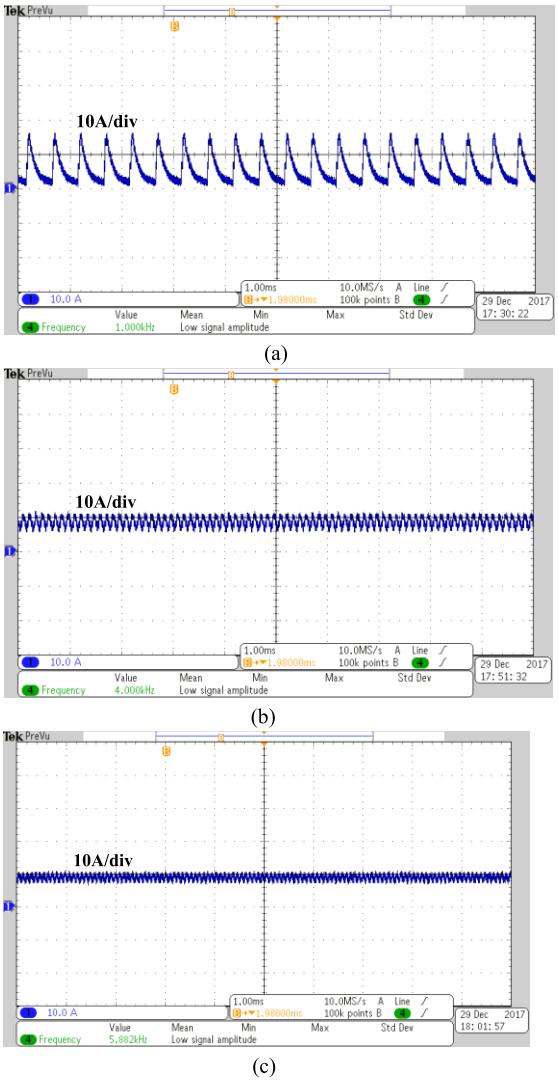

FIGURE 11. Waveforms of input current with variable switching frequency (1kHz, 6kHz and 10kHz) and 500Ω load resistance. (a) f_{sq}=1kHz, R_L=500Ω. (b) f_{sq}=6kHz, R_L=500Ω. (c) f_{sq}=10kHz, R_L=500Ω.

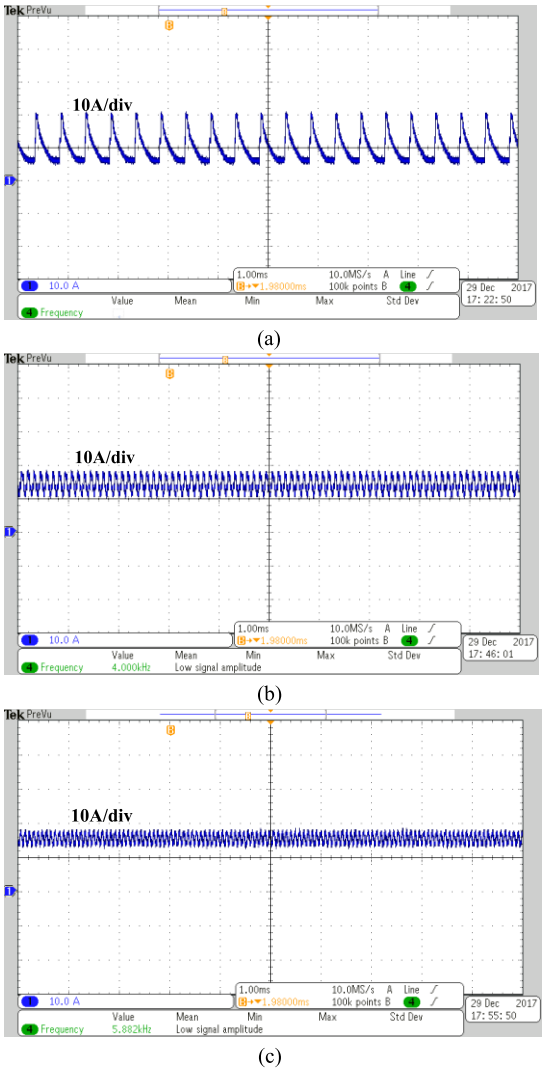

FIGURE 12. Waveforms of input current with variable switching frequency (1kHz, 6kHz and 10kHz) and 250Ω load resistance. (a) f_{sq}=1kHz, R_L=250Ω. (b) f_{sq}=6kHz, R_L=250Ω. (c) f_{sq}=10kHz, R_L=250Ω.

By injecting the 10uH inductor in the charge loop of the proposed SC converter, it achieves the continuous input current. The theory analysis is verified by the simulated results. The voltage conversion ratio is about 10 at the load resistance 500Ω and the switching frequency 6 kHz. As a result, the high conversion ratio and good performance of the proposed converter is verified in the variable operation conditions. What's more, the high voltage ripples in the low switching frequency condition in the proposed circuit could be avoided by applying the feedback loop control method and optimizing the circuit. By adjusting the switching frequency, it can get the different voltage conversion ratio. For the proposed isolated SC converter, the boundary switching frequency should be considered for the regulation. If the switching frequency is set under the boundary switching frequency, the higher switching frequency can produce the higher voltage gain ratio as shown in Fig.7. However, if the switching frequency is set over the boundary switching frequency, the higher switching frequency will get the lower voltage gain ratio as shown in Fig.7.

C. EXPERIMENTAL RESULTS

The experiment and simulation share the same parameters of the proposed isolated SC converter as shown in Table 1. The steady-state and the dynamic experiments are done. Fig.8 and Fig.9 show the performance of the proposed isolated SC converter with the switching frequency 1kHz,6kHz and 10kHz and the load resistance 500Ω and 250Ω. Fig.10 shows the dynamic response with the load current step-up and load power step-down. Fig.11 and Fig.12 respectively show the input current under load resistance 500Ω and 250Ω with the switching frequency 1kHz,6kHz and 10kHz. As shown in Fig.8 and Fig.9, the experimental results demonstrates the high conversion ratio and the stable performance of the proposed isolated SC converter with variable operating conditions. By changing the switching frequency, the different

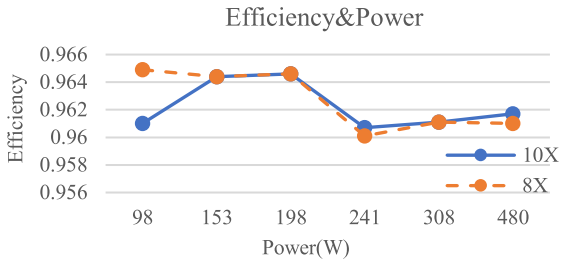

FIGURE 13. Efficiency of 8X and 10X proposed converter with the variable power levels.

voltage gain ratio can be achieved. The output voltage and the load current are maintained stable. It can be seen from Fig.8 and Fig.9, the maximum gain ratio of the proposed ITBRSC converter is about 10 under the load resistance 500 Ω and switching frequency 6kHz. The experimental result is same to the simulated result. As shown in Fig.10, with the variable load resistance, the output voltage will change immediately at the transient point. Fig.11 and Fig.12 show that the proposed isolated SC converter achieves the continuous input current with the help of the small value inductor L_1. In the higher switching frequency condition, the ripple of the input current will be lower. As a result, the experimental results agree very well with the simulated results.

D. EFFICIENCY

In this paper, the energy efficiency of the proposed isolated SC converter is measured with the 8X and 10X voltage gain ratios. The maximum power of the proposed isolated SC converter is 480W. The switching frequency is set 10kHz. Fig.13 shows that, it achieves the high energy efficiency in both the 8X model and 10X model. The peak efficiency of the proposed converter is 96.5% under all tested data. It is achieved at 98W condition with the 8X isolated SC proposed converter. By adopting the high band-gap devices and optimizing the transformer and power circuit, the energy efficiency of the proposed ITBRSC could be further improved in the future work. The output voltage regulation or load current regulation could be reached with the closed-loop control method.

The proposed isolated SC converter is built with the simple topology. The cost is lower than the inductor-based high gain isolated converter. This isolated SC converter could be constructed with high-power density and small volume. Thanks to the small value inductors in the charge loop and discharge loop, the current spikes are much smaller than the general SC converter with the lower EMI noise.

V. CONCLUSIONS AND DISCISSONS

This paper proposes a high gain ratio isolated ITBRSC converter. This SC converter is constructed by optimizing TBRSC converter cell and by pioneering the isolation function for the TBRSC converter. By injecting the two small value inductors in the charge loop and discharge loop, the pulsating current is highly reduced, and the continuous input current is realized. A 500W ITBRSC converter is constructed for the experimental verification. The high voltage conversion ratio is verified with the proposed isolated SC converter. The simulated and experimental results both demonstrate that the feasibility of design and good performance of the proposed isolated SC converter. The ITBRSC topology could be used in the high gain isolated boosting converter application areas for the sustainable energy applications which focus on the high gain ratio and the isolation function. In the future work, the authors will conduct the research on the high-power ITBRSC converter with the high switching frequency and the high-power density.

REFERENCES

[1] H. Taghizadeh, A. M. Cross, R. Whitehouse, and C. Barker, "An algorithm for automatically calculating component current ratings in switched-capacitor DC-DC converters," *IEEE Access*, vol. 6, pp. 15702–15712, 2018.

[2] F. Shang, G. Niu, and M. Krishnamurthy, "Design and analysis of a high-voltage-gain step-up resonant DC–DC converter for transportation applications," *IEEE Trans. Transport. Electrific.*, vol. 3, no. 1, pp. 157–167, Mar. 2017.

[3] L. Yang, J. Zhang, W. Yu, X. Tong, and X. Wu, "Analysis of isolated high boost quasi-two switch boosting switched-capacitor converter," in *Proc. 13th IEEE Conf. Ind. Electron. Appl. (ICIEA)*, May/Jun. 2018, pp. 281–286.

[4] S. M. Salehi, S. M. Dehghan, and S. Hasanzadeh, "Interleaved-input series-output ultra high voltage gain DC-DC converter," *IEEE Trans. Power Electron.*, to be published, doi: 10.1109/TPEL.2018.2853577.

[5] Y. Lu, J. Jiang, and W.-H. Ki, "Design considerations of distributed and centralized switched-capacitor converters for power supply on-chip," *IEEE Trans. Emerg. Sel. Topics Circuits Syst.*, vol. 6, no. 2, pp. 515–525, Jun. 2018.

[6] M. Uno, K. Yashiro, and K. Hasegawa, "Modularized equalization architecture with voltage multiplier-based cell equalizer and switchless switched capacitor converter-based module equalizer for series-connected electric double-layer capacitors," *IEEE Trans. Power Electron.*, to be published, doi: 10.1109/TPEL.2018.2876061.

[7] R. L. da Silva, T. B. Lazzarin, and I. Barbi, "Reduced switch count step-up/step-down switched-capacitor three-phase AC–AC converter," *IEEE Trans. Power Electron.*, vol. 65, no. 11, pp. 8422–8432, Nov. 2018.

[8] M. P. Shreelakshmi, M. Das, and V. Agarwal, "Design and development of a novel high voltage gain, high efficiency bi-directional DC-DC converter for storage interface," *IEEE Trans. Ind. Electron.*, to be published, doi: 10.1109/TIE.2018.2860539.

[9] T. Sai, Y. Yamauchi, H. Kando, T. Funaki, T. Sakurai, and M. Takamiya, "2/3 and 1/2 reconfigurable switched capacitor DC–DC converter with 92.9% efficiency at 62 mW/mm^2 using driver amplitude doubler," *IEEE Trans. Circuits Syst. II, Exp. Briefs*, vol. 65, no. 11, pp. 1654–1658 , Nov. 2018.

[10] D. Kilani, M. Alhawari, B. Mohammad, H. Saleh, and M. Ismail, "An efficient and small area multioutput switched capacitor buck converter for IoTs," in *Proc. IEEE Int. Symp. Circuits Syst. (ISCAS)*, May 2018, pp. 1–4.

[11] D. Kilani, M. Alhawari, B. Mohammad, H. Saleh, and M. Ismail, "An efficient switched-capacitor DC-DC buck converter for self-powered wearable electronics," *IEEE Trans. Circuits Syst. I, Reg. Papers*, vol. 63, pp. 1557–1566, Oct. 2016.

[12] V. E. Shunkov, O. N. Kus, V. Y. Prokopyev, V. A. Butuzov, and Y. I. Bocharov, "Fully integrated switched-capacitor voltage converter with regulated output," in *Proc. Moscow Workshop Electron. Netw. Technol. (MWENT)*, 2018, pp. 1–4.

[13] K.-H. Chen, "A fully integrated asymmetrical shunt switched-capacitor DC-DC converter with fast optimum ratio searching scheme for load transient enhancement," *IEEE Trans. Power Electron.*, to be published, doi: 10.1109/TPEL.2018.2889870.

[14] T. M. Andersen *et al.*, "A sub-ns response on-chip switched-capacitor DC-DC voltage regulator delivering 3.7 W/mm^2 at 90% efficiency using deep-trench capacitors in 32 nm SOI CMOS," in *IEEE Int. Solid-State Circuits Conf. (ISSCC) Dig. Tech. Papers*, Feb. 2014, pp. 90–91.
[15] T. Tong, S. K. Lee, X. Zhang, D. Brooks, and G.-Y. Wei, "A fully integrated reconfigurable switched-capacitor DC-DC converter with four stacked output channels for voltage stacking applications," *IEEE J. Solid-State Circuits*, vol. 51, no. 9, pp. 2142–2152, Sep. 2016.
[16] A. Biswas, Y. Sinangil, and A. P. Chandrakasan, "A 28 nm FDSOI integrated reconfigurable switched-capacitor based step-up DC-DC converter with 88% peak efficiency," *IEEE J. Solid-State Circuits*, vol. 50, no. 7, pp. 1540–1549, Jul. 2015.
[17] R. Jain *et al.*, "A 0.45–1 V fully-integrated distributed switched capacitor DC-DC converter with high density MIM capacitor in 22 nm tri-gate CMOS," *IEEE J. Solid-State Circuits*, vol. 49, no. 4, pp. 917–927, Apr. 2014.
[18] N. Butzen and M. Steyaert, "Design of single-topology continuously scalable-conversion-ratio switched-capacitor DC-DC converters," *IEEE J. Solid-State Circuits*, to be published, doi: 10.1109/JSSC.2018.2884351.
[19] A. Kawa, R. Stala, A. Mondzik, S. Pirog, and A. Penczek, "High-power thyristor-based DC–DC switched-capacitor voltage multipliers: Basic concept and novel derived topology with reduced number of switches," *IEEE Trans. Power Electron.*, vol. 31, no. 10, pp. 6797–6813, Oct. 2016.
[20] W. Qian, H. Cha, F. Z. Peng, and L. M. Tolbert, "55-kW variable 3X DC-DC converter for plug-in hybrid electric vehicles," *IEEE Trans. Power Electron.*, vol. 27, no. 4, pp. 1668–1678, Apr. 2012.
[21] A. Parastar and J.-K. Seok, "High-gain resonant switched-capacitor cell-based DC/DC converter for offshore wind energy systems," *IEEE Trans. Power Electron.*, vol. 30, no. 2, pp. 644–656, Feb. 2015.
[22] M. Wang, X. Yang, L. Wang, and T. Q. Zheng, "Resonant switched capacitor converter based DC auto-transformer for urban rail transit," in *Proc. IEEE Appl. Power Electron. Conf. Expo. (APEC)*, Mar. 2018, pp. 1441–1446.
[23] K. Zou, M. J. Scott, and J. Wang, "A switched-capacitor voltage tripler with automatic interleaving capability," *IEEE Trans. Power Electron.*, vol. 27, no. 6, pp. 2857–2868, Jun. 2012.
[24] R. L. Andersen, T. B. Lazzarin, and I. Barbi, "A 1-kW step-up/step-down switched-capacitor AC–AC converter," *IEEE Trans. Power Electron.*, vol. 28, no. 7, pp. 3329–3340, Jul. 2013.
[25] H. Setiadi and H. Fujita, "Control and performance of new asymmetrical operation for switched-capacitor-based resonant converters," in *Proc. Int. Power Electron. Conf. (IPEC-Niigata-ECCE Asia)*, 2018, pp. 626–631.
[26] F. Zhang, L. Du, F. Z. Peng, and Z. Qian, "A new design method for high-power high-efficiency switched-capacitor DC–DC converters," *IEEE Trans. Power Electron.*, vol. 23, no. 2, pp. 832–840, Mar. 2008.
[27] M. Martins, M. S. Perdigão, A. S. Mendes, R. A. Pinto, and J. M. Alonso, "Dimmable LED driver with variable inductor based on a resonant switched-capacitor topology," in *Proc. Energy Convers. Congr. Expo.*, 2015, pp. 5329–5336.
[28] C. Zhao, X. Xie, and S. Liu, "Multioutput LED drivers with precise passive current balancing," *IEEE Trans. Power Electron.*, vol. 28, no. 3, pp. 1438–1448, Mar. 2013.
[29] W. Feng and F. G. Shi, "A new switched-capacitor frequency modulated driver for light emitting diodes," *Rev. Sci. Instrum.*, vol. 78, no. 11, pp. 1147011–1147014, Nov. 2007.
[30] E. E. dos Santos Filho, P. H. A. Miranda, E. M. Sá, and F. L. M. Antunes, "A LED driver with switched capacitor," *IEEE Trans. Ind. Appl.*, vol. 50, no. 5, pp. 3046–3054, Sep./Oct. 2014.
[31] C. Yue, Y. Lei, R. C. N. Pilawa-Podgurski, and P. T. Krein, "Modular switched-capacitor DC-DC converters tied with lithium-ion batteries for use in battery electric vehicles," in *Proc. Energy Convers. Congr. Expo.*, 2015, pp. 85–91.
[32] M. Chen, K. K. Afridi, and D. J. Perreault, "Stacked switched capacitor energy buffer architecture," *IEEE Trans. Power Electron.*, vol. 28, no. 11, pp. 5183–5195, Nov. 2013.
[33] Z. Amjadi and S. S. Williamson, "Modeling, simulation, and control of an advanced Luo converter for plug-in hybrid electric vehicle energy-storage system," *IEEE Trans. Veh. Technol.*, vol. 60, no. 1, pp. 64–75, Jan. 2011.
[34] Z. Amjadi and S. S. Williamson, "A novel control technique for a switched-capacitor-converter-based hybrid electric vehicle energy storage system," *IEEE Trans. Ind. Electron.*, vol. 57, no. 3, pp. 926–934, Mar. 2010.
[35] B. Wu, S. Li, K. M. Smedley, and S. Singer, "A family of two-switch boosting switched-capacitor converters," *IEEE Trans. Power Electron.*, vol. 30, no. 10, pp. 5413–5424, Oct. 2015.
[36] B. Wu, S. Keyue, and S. Sigmond, "A new 3X interleaved bidirectional switched capacitor converter," in *Proc. IEEE Appl. Power Electron. Conf. Expo.*, Mar. 2014, pp. 1433–1439.
[37] B. Wu, S. Li, K. M. Smedley, and S. Singer, "Analysis of high-power switched-capacitor converter regulation based on charge-balance transient-calculation method," *IEEE Trans. Power Electron.*, vol. 31, no. 5, pp. 3482–3494, May 2015.
[38] L. Yang, W. Zhang, X. Zhang, and G. P. Li, "Nonlinear variable frequency control of high power switched-capacitor converter," in *Proc. IPEMC*, 2016, pp. 3472–3476.
[39] X. Zhang, C. Yao, C. Li, L. Fu, F. Guo, and J. Wang, "A wide bandgap device-based isolated quasi-switched-capacitor DC/DC converter," *IEEE Trans. Power Electron.*, vol. 29, no. 5, pp. 2500–2510, May 2014.
[40] X. Zhang, C. Yao, and J. Wang, "A quasi-switched-capacitor resonant converter," *IEEE Trans. Power Electron.*, vol. 31, no. 11, pp. 7849–7856, Nov. 2016.
[41] X. Zhang, F. Guo, C. Yao, H. Li, P. Xu, and J. Wang, "Small-signal modeling and controller design of an isolated quasi-switched-capacitor DC/DC converter," in *Proc. IEEE Appl. Power Electron. Conf. Expo.*, Mar. 2014, pp. 1032–1038.
[42] H.-W. Kim and J.-H. Park, "Isolated bidirectional switched-capacitor flyback converter," in *Proc. IEEE Power Electron. Appl. Conf. Expo.*, Nov. 2015, pp. 279–284.
[43] S. Li, Y. Zheng, B. Wu, and K. M. Smedley, "A family of resonant two-switch boosting switched-capacitor converter with ZVS operation and a wide line regulation range," *IEEE Trans. Power Electron.*, vol. 33, no. 1, pp. 448–459, Jan. 2018.
[44] J. M. Henry and J. W. Kimball, "Practical performance analysis of complex switched-capacitor converters," *IEEE Trans. Power Electron.*, vol. 26, no. 1, pp. 127–136, Jan. 2011.
[45] J. M. Henry and J. W. Kimball, "Switched-capacitor converter state model generator," *IEEE Trans. Power Electron.*, vol. 27, no. 5, pp. 2415–2425, May 2012.
[46] M. Evzelman and S. Ben-Yaakov, "Average-current-based conduction losses model of switched capacitor converters," *IEEE Trans. Power Electron.*, vol. 28, no. 7, pp. 3341–3352, Jul. 2013.
[47] S. Ben-Yaakov, "Behavioral average modeling and equivalent circuit simulation of switched capacitors converters," *IEEE Trans. Power Electron.*, vol. 27, no. 2, pp. 632–636, Feb. 2012.
[48] M. D. Seeman and S. R. Sanders, "Analysis and optimization of switched-capacitor DC-DC converters," *IEEE Trans. Power Electron.*, vol. 23, no. 2, pp. 841–851, Mar. 2008.
[49] L. Müller and J. W. Kimball, "A dynamic model of switched-capacitor power converters," *IEEE Trans. Power Electron.*, vol. 29, no. 4, pp. 1862–1869, Apr. 2014.
[50] L. Yang, B. Wu, X. Tong, K. M. Smedley, and G.-P. Li, "Dynamic capacitor ampere-second balance transient calculation modeling method for switched-capacitor converters," *IEEE Trans. Power Electron.*, vol. 33, no. 10, pp. 8916–8926, Oct. 2018.
[51] B. Wu, L. Yang, X. Zhang, K. M. Smedley, and G.-P. Li, "Modeling and analysis of variable frequency one-cycle control on high-power switched-capacitor converters," *IEEE Trans. Power Electron.*, vol. 33, no. 6, pp. 5465–5475, Jun. 2018.
[52] L. Yang, B. Wu, X. Zhang, K. Smedley, and G.-P. Li, "Dynamic modeling and analysis of constant on time variable frequency one-cycle control for switched-capacitor converters," *IEEE Trans. Circuits Syst. I, Reg. Papers*, vol. 64, no. 3, pp. 630–641, Mar. 2017.

LEI YANG (S'15–M'17) was born in Henan, China, in 1986. He received the B.S degree in electric and information engineering from Information Engineering University, Zhengzhou, China, in 2011, and the M.S. degree in signal and information processing and the Ph.D. degree in electrical engineering from Northwestern Polytechnical University, Xi'an, Shaanxi, China, in 2014 and 2017, respectively. From 2014 to 2016, he was a Visiting Student with the University of California at Irvine, Irvine, CA, USA. He is currently an Assistant Professor with Xi'an University of Technology.

His research interests include nonlinear control, switched-capacitor converter, dc–dc converter, power source of electrical vehicle, wireless power and data transfer systems, and renewable energy integration.

WENQIAN YU (S'17) was born in Shaanxi, China, in 1995. She received the B.S degree in electrical engineering from the Xi'an University of Technology, Xi'an, China, in 2017, where she is currently pursuing the master's degree.

Her research interests include nonlinear control, active power filter, switched-capacitor converter, and dc–dc converter.

JIAXIANG ZHANG (S'17) was born in Shaanxi, China, in 1994. He is currently pursuing the master's degree in electrical engineering with the Xi'an University of Technology.

His research interests include bidirectional-dc/dc converter, nonlinear control method, switched-capacitor converter, dc–dc converter, power source of electrical vehicle, and ac/dc hybrid microgrid.